International Journal of Nanomedicine

Dovepress
open access to scientific and medical research

Open Access Full Text Article

ORIGINAL RESEARCH

Preparation, in vitro and in vivo evaluation of polymeric nanoparticles based on hyaluronic acid-poly(butyl cyanoacrylate) and D-alpha-tocopheryl polyethylene glycol 1000 succinate for tumor-targeted delivery of morin hydrate

This article was published in the following Dove Press journal:
International Journal of Nanomedicine
6 January 2015
Number of times this article has been viewed

Sarra Abbad[1,2]
Cheng Wang[1]
Ayman Yahia Waddad[1]
Huixia Lv[1]
Jianping Zhou[1]

[1]Department of Pharmaceutics, China Pharmaceutical University, Nanjing, People's Republic of China; [2]Department of Pharmacy, Abou Bekr Belkaid University, Tlemcen, Algeria

Abstract: Herein, we describe the preparation of a targeted cellular delivery system for morin hydrate (MH), based on a low-molecular-weight hyaluronic acid-poly(butyl cyanoacrylate) (HA-PBCA) block copolymer. In order to enhance the therapeutic effect of MH, D-alpha-tocopheryl polyethylene glycol 1000 succinate (TPGS) was mixed with HA-PBCA during the preparation process. The MH-loaded HA-PBCA "plain" nanoparticle (MH-PNs) and HA-PBCA/TPGS "mixed" nanoparticles (MH-MNs) were concomitantly characterized in terms of loading efficiency, particle size, zeta potential, critical aggregation concentration, and morphology. The obtained MH-PNs and MH-MNs exhibited a spherical morphology with a negative zeta potential and a particle size less than 200 nm, favorable for drug targeting. Remarkably, the addition of TPGS resulted in about 1.6-fold increase in drug-loading. The in vitro cell viability experiment revealed that MH-MNs enhanced the cytotoxicity of MH in A549 cells compared with MH solution and MH-PNs. Furthermore, blank MNs containing TPGS exhibited selective cytotoxic effects against cancer cells without diminishing the viability of normal cells. In addition, the cellular uptake study indicated that MNs resulted in 2.28-fold higher cellular uptake than that of PNs, in A549 cells. The CD44 receptor competitive inhibition and the internalization pathway studies suggested that the internalization mechanism of the nanoparticles was mediated mainly by the CD44 receptors through a clathrin-dependent endocytic pathway. More importantly, MH-MNs exhibited a higher in vivo antitumor potency and induced more tumor cell apoptosis than did MH-PNs, following intravenous administration to S180 tumor-bearing mice. Overall, the results imply that the developed nanoparticles are promising vehicles for the targeted delivery of lipophilic anticancer drugs.

Keywords: anti-tumor effect, hyaluronic acid, TPGS, morin hydrate, nanoparticles

Introduction

Morin hydrate (3,5,7,2′,4′-pentahydroxyflavone) (MH), a naturally occurring bioflavonoid identified in a number of fruits, vegetables, and herbs of the *Moraceae* family, is emerging as a potent therapeutic drug for different maladies, including cardiovascular disease, diabetes mellitus, neurodegenerative disease, cancer, and inflammation.[1,2] This flavonoid has been reported to induce apoptosis in a hepatocellular carcinoma model and human cultured prostate cancer cells.[3,4] Additionally, it inhibits the growth of HL-60 cells and breast cancer-resistance protein (ABCG2)-mediated transport.[5,6]

Correspondence: Huixia Lv/Jianping Zhou
Department of Pharmaceutics, China Pharmaceutical University, 24 Tongjiaxiang, Nanjing 210009, People's Republic of China
Tel +86 25 8327 1272
Fax +86 25 8330 1606
Email lvhuixia@163.com/jianpingzhoucpu@yahoo.com

In spite of the research progress made on the pharmacological activity of MH, only two formulation techniques have been developed to improve the bioavailability of the poorly water-soluble MH: a self-nanoemulsifying MH delivery system based on the phospholipid complex technique reported by Zhang et al[1] and a niosomal dispersion composed of nonionic surfactants (Span 60, Span 80, and Tween 60) developed by our group.[7]

The use of biocompatible polymer in the treatment of various ailments has widely expanded over the past decade, among which hyaluronic acid (HA), a naturally occurring polyanionic unbranched polysaccharide, has been implicated in several biological functions, such as cell adhesion and motility, cell proliferation and differentiation, wound healing, and even cancer metastasis.[8,9] More importantly, the overexpression of HA-binding receptors, such as CD44 and RHAMM, has been found on the cell surface of several malignant tumors,[10] and data showed that the interaction of hyaluronan with its cell surface receptors is crucial for tumor progression.[11] Aside from these properties and unlike dextran and pullulan, HA has demonstrated a weaker specificity toward hepatic receptors, contributing to an enhanced accumulation of HA nanoparticles in tumor sites.[12] Based on these points, HA and its derivatives have been popularly used as active tumor-targeting vehicles for various anticancer drugs. The importance of HA has elicited research directed toward developing methodology for its chemical modification and conjugation, mainly by targeting its reactive functionalities, such as carboxylic groups, hydroxyl groups, and the HA reducing end.[13,14] HA-based brush copolymers have been widely applied to obtain a large variety of nanoparticles, whereas HA-based block copolymers are more scarce and appealing. Many research groups have already worked on the synthesis of HA block copolymers, via different coupling methods; for instance, the HA-poly(butyl cyanoacrylate) (HA-PBCA) block copolymer, previously reported by He et al was prepared through redox radical emulsion polymerization.[15] However, polymeric nanoparticles formed from a single polymer often lack multiple functionalities, due to the limitation in the number of building blocks. In order to overcome this limitation, the polymeric nanoparticles consisting of more than one amphiphilic polymer have aroused great interest recently.[16] Based on the advantages of the mixed polymeric nanoparticles (MNs) over simple polymeric nanoparticles (PNs), a large number of MNs have been designed and found to be superior to their individual constituents.[17] So herein, we report the first attempt on the combination of HA-based block copolymer with vitamin E derivatives (Figure 1A).

The D-alpha-tocopheryl polyethylene glycol 1000 succinate (TPGS) is a water-soluble derivative of natural vitamin E.[18] It has been widely applied in the food and drug industry as an absorption enhancer and as a drug solubilizer in oral, parenteral, topical, nasal, and rectal/vaginal therapies, and is gaining interest in the development of novel drug delivery formulations.[19,20] TPGS is usually mixed with other biodegradable materials in the preparation of nanoparticles, to enhance the aqueous solubility of hydrophobic molecules.[21] It can inhibit the multidrug resistance transporter, P-glycoprotein (P-gp), thus increasing the oral bioavailability of many anticancer drugs. TPGS can also greatly improve the performance of TPGS-emulsified nanoparticles, leading to enhanced cellular uptake and in vitro cancer cell mortality, and more desirable in vivo pharmacokinetics.[22,23] In addition, TPGS has been reported to efficiently inhibit the growth of human lung cancer cells both in vivo and in vitro.[24] Furthermore, TPGS produces synergistic growth inhibition effects upon combination with other anticancer drugs due to its ability to induce apoptosis in tumor cells.[25]

Although there have been many HA-based PNs exploited for drug delivery, this is the first report on the formulation of a multifunctional drug delivery system based on HA block copolymer and TPGS. We hypothesized that MNs made of HA-PBCA and TPGS may allow for a better drug encapsulation, a higher stability, and a stronger anticancer activity. Our study focuses on combining functional homopolymers in a single delivery system that can reach the tumor passively through the leaky surrounding vasculature by the enhanced permeability and retention effect (EPR) of TPGS, and actively through the binding of HA to the receptors overexpressed by cancer cells or angiogenic endothelial cells (as shown in Figure 1B). TPGS can further increase the cellular uptake owing to its bioadhesive properties. In the present work, we describe the preparation of MH-PNs and MH-MNs as carriers for targeted delivery of MH. The prepared formulations were characterized for their particle size, zeta potential, entrapment efficiency, and drug-loading (DL). The in vitro cellular uptake, the receptor-mediated tumor-targeting characteristics, and the cytotoxicity were evaluated against the human A549 lung adenocarcinoma cell line. Here, the study aimed to unveil whether TPGS could synergistically increase the cytotoxicity of MH. Finally, the antitumor efficacy of MH-loaded nanoparticles against S180 tumor xenograft models was evaluated.

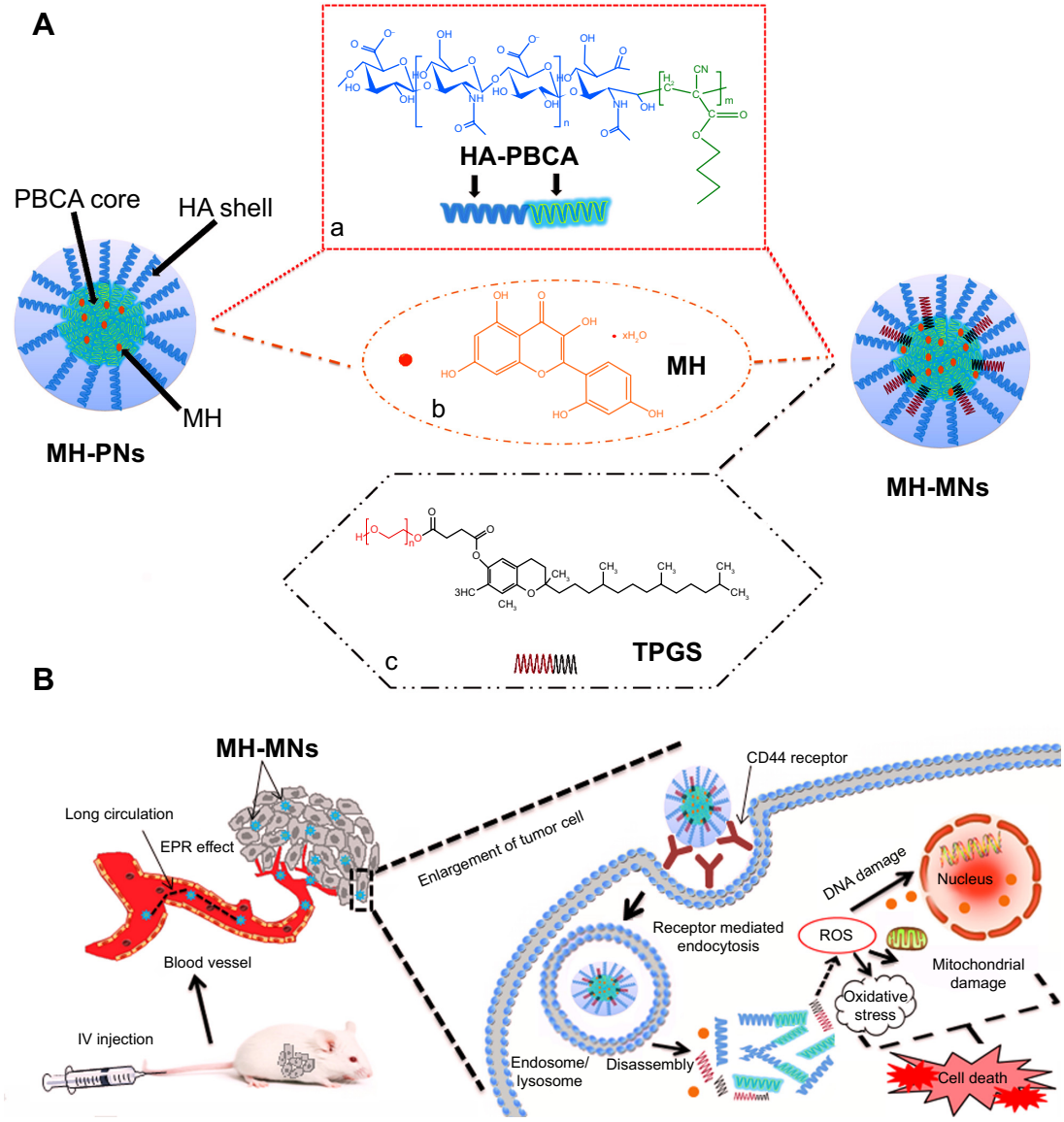

Figure 1 Schematic illustration of (**A**) the core–shell structure of MH-PNs and MH-MNs, and (**B**) accumulation of nanoparticles in tumor sites through the EPR effect, intracellular trafficking pathway, and synergistic antitumor effect of MH and TPGS.

Notes: Chemical structures of HA-PBCA (a), MH (b), and TPGS (c). The intracellular trafficking pathway includes steps of receptor-meditated cellular internalization, endolysosomal disassembly, and drug release.

Abbreviations: EPR, enhanced permeability and retention; HA-PBCA, hyaluronic acid-poly(butyl cyanoacrylate); IV, intravenous; MH, morin hydrate; MH-MNs, morin hydrate-loaded mixed nanoparticles; MH-PNs, morin hydrate-loaded plain nanoparticles; ROS, reactive oxygen species; TPGS, D-alpha-tocopheryl polyethylene glycol 1000 succinate.

Materials and methods

Materials

Sodium HA (molecular weight [MW] =10 kDa) was purchased from Zhenjiang Dong Yuan Biotech Company Co., Ltd (Zhenjiang, People's Republic of China). Butyl cyanoacrylate (BCA) monomers were obtained from Suncon Medical Adhesive Company (Beijing, People's Republic of China). MH, TPGS, 3-[4,5-dimethylthiazol-2-yl]-2,5-diphenyl-tetrazolium bromide (MTT), nystatin, and amiloride were purchased from Sigma-Aldrich Corp (St Louis, MO, USA). Propidium iodine (PI) was purchased from Beyotime Biotechnology (Nanjing, People's Republic of China). All other solvents and chemicals used were of high-performance liquid chromatography (HPLC) and analytical grades.

Cell lines and cell culture

Human lung adenocarcinoma (A549) and human hepatic (L02) cell lines were purchased from American Type Culture Collection (ATCC) (Manassas, VA, USA). Cells were maintained in Roswell Park Memorial Institute

(RPMI)-1640 medium supplemented with 10% (v/v) heat-inactivated fetal bovine serum (FBS), 2 mM glutamine, 10 mM 4-(2-hydroxyethyl)-1-piperazineethanesulfonic acid (HEPES) buffer, 100 U/mL streptomycin, and 100 U/mL penicillin at 37°C in a humid atmosphere (5% CO_2, 95% air). For subculture, cells were detached with 0.25% trypsin-ethylenediaminetetraaceticacid (EDTA) solution, and seeded into new flasks.

Synthesis and characterization of HA-PBCA

HA-PBCA was synthesized as described previously by He et al[15] with a little modification. Briefly, 0.1 g of HA was dissolved in 9 mL of nitric acid (0.2 mol/L) at 40°C and stirred for 10 minutes under nitrogen bubbling. Ammonium cerium nitrate (0.8 mmol/L) solution in 1 mL nitric acid (0.2 M) and BCA were successively added under vigorous agitation. Nitrogen bubbling was maintained for 10 minutes. Then the reaction was left to continue under gentle stirring for another 50 minutes. Reactants were transferred into a dialysis membrane (MW cutoff [MWCO], 3,500 Da) and were exhaustively dialyzed against water for 3 days. The suspension was lyophilized for 2 days and then stored at 4°C for further use.

Preparation of MH-PNs and MH-MNs

MH-PNs and MH-MNs were prepared by a probe-type ultrasonic and dialysis method as previously described by Li et al.[9] Briefly, 15 mg of HA-PBCA copolymer was dissolved in 3 mL of phosphate-buffered saline (PBS) pH 7.4, then MH in 0.5 mL dimethyl sulfoxide DMSO was added dropwise to the polymer suspension, under stirring at 150 rpm at room temperature; the final mixture was ultrasonicated for 30 minutes in an ice bath by a probe-type ultrasonicator (JY92-2D; Ningbo Scientz Biotechnology Co., Ltd, Nanjing, People's Republic of China). The solution was dialyzed against excess amount of distilled water for 12 hours using a dialysis bag with MWCO of 3,500 Da, followed by filtration through a 0.45 μm pore-sized microporous membrane and lyophilization. MH-MNs were prepared similarly, except HA-PBCA solution was replaced by a mixture of HA-PBCA and TPGS (15 mg/mL TPGS solution in PBS pH 7.4 was used) at different weight ratios.

Critical aggregation concentration (CAC) determination

The CAC was determined by fluorescence spectroscopy using pyrene as a hydrophobic probe.[26] Briefly, 1 mL of 6.0×10^{-6} M pyrene solution in acetone was added to a series of 10 mL volumetric flasks, and acetone was subsequently completely evaporated under a gentle nitrogen gas stream for 1 hour at 60°C. HA-PBCA and TPGS at different weight ratios, with concentrations ranging from 0.000001 to 1.0 mg/mL, were added to each tube to achieve a final pyrene concentration of 6.0×10^{-7} M, followed by sonication for 30 minutes. The samples were incubated at 50°C for 1 hour and then left to cool down overnight at room temperature. Fluorescence spectra were obtained using a fluorescence spectrophotometer (RF-5301 PC; Shimadzu Corp, Kyoto, Japan) at an emission wavelength of 390 nm and slit widths of 3 nm for both excitation and emission. The CAC was estimated as the cross point when extrapolating the intensity ratio I338/I333 at low and high concentration regions.

Morphology, particle size, and zeta potential analysis

The particle size and polydispersity index were assessed by dynamic light scattering (DLS) (NanoBrook 90Plus Particle Size Analyzer; Brookhaven Instruments Corp, New York, NY, USA) at 25.0°C±0.1°C by measuring the autocorrelation function at 90°. The mean size and standard error were directly measured by the instrument fitting data. The zeta potential of the nanoparticles was determined using a Zeta plus zeta potential analyzer (Brookhaven Instruments Corp) at 25°C. Each experiment was carried out in triplicate. The morphologies and size distributions were observed by transmission electron microscopy (TEM) under a JEM-2100 Electron Microscope (JEOL, Tokyo, Japan) at an accelerating voltage of 80 kV. A drop of nanoparticle suspension was placed onto a copper grid and left to adhere for 2 minutes. The excess suspension was wicked off with a filter paper, and air-dried before observation.

Drug-loading and encapsulation efficiency

The nanoparticles solution was suitably diluted with ethanol (20 times) and sonicated for 30 minutes (KQ-250 Ultrasound Sonificator; Kunshan Ultrasound Instrument Co., Ltd, Kunshan, People's Republic of China), then centrifuged at 12,000 rpm for 10 minutes at 4°C. The MH content in the supernatant was assayed by HPLC (Shimadzu LC-2010 CHT system; Shimadzu Corp) equipped with an XTerra MS C18 reversed-phase column (250×4.6 mm, 5 μm) used in isocratic mode at 30°C. The mobile phase consisted of a mixture of acetonitrile and 10 mM KH_2PO_2 (28:72, v/v) at pH 2 (phosphoric acid) with a flow rate of 1.0 mL/min. Detection

was performed at a wavelength of 260 nm, and the injection volume for samples was 20 µL.[7] The standard curve was linear and ranged from 1 to 100 µg/mL, with a correlation coefficient (R^2) value of 0.9999. The accuracy was determined by three replicate injections of three different concentrations of MH, and a percent accuracy and relative standard deviation of repeatability found to be between 99.31% and 100.67% and less than 2%, respectively. Therefore, validation studies revealed that the proposed method is suitable for determination of MH concentration in MH nanoparticles.

The entrapment efficiency (EE) and DL were calculated using the following equations:

$$\text{EE}\,(\%) = \frac{\text{Weight of MH in polymeric nanoparticles}}{\text{Weight of MH fed initially}} \times 100 \quad (1)$$

$$\text{DL}\,(\%) = \frac{\text{Weight of MH in polymeric nanoparticles}}{\text{Weight of polymeric nanoparticles}} \times 100 \quad (2)$$

Differential scanning calorimetry

Differential scanning calorimetry (DSC) of the samples was performed using a NETZSCH DSC 204 (Bavaria, Germany). Samples were heated from ambient temperature to 300°C at a constant heating rate of 10°C/min under a nitrogen atmosphere.

In vitro cytotoxicity studies

In vitro cytotoxicity of the blank nanoparticles was evaluated by the MTT assay. Briefly, A549 and L02 cells were seeded at a density of 5×10^3 cells per well in 96-well plates and cultured overnight at 37°C in 200 µL of RPMI-1640 supplemented with 10% FBS. Afterwards, the culture medium was removed, and the cells were incubated for 72 hours in a serum-free medium containing blank nanoparticles at various concentrations. Then, 20 µL of MTT solution (5 mg/mL) was added to each well, and the cells were further incubated for 4 hours. The supernatant in the wells was discarded, and 150 µL of DMSO was added to dissolve the substrate, for 10 minutes. The absorbance in each well was recorded at 570 nm using a microplate reader (Bio-Rad Laboratories, Hercules, CA, USA). This experiment was performed thrice.

The cytotoxicity of MH-loaded nanoparticles was evaluated by staining nonviable cells with PI.[27] The assay was conducted according to the manufacturer's protocol. Briefly, cells in 12-well plates were incubated with increasing concentrations of free MH, MH-PNs, or MH-MNs. The culture medium without any formulation was used as the control. Afterwards, the cells were washed with PBS and harvested by trypsinization. Culture medium supplemented with 10% FBS was added to stop the trypsin action, followed by centrifugation and resuspension in cold PBS, twice. Then, 20 µL of PI (10 µg/mL in PBS pH 7.4) was then added to 200 µL of the cellular suspension. The numbers of necrotic cells were immediately evaluated with a flow cytometer (FCM) (BD FACSCalibur™; BD Biosciences, Franklin Lakes, NJ, USA).

In vitro cellular uptake

Fluorescence microscopy

To evaluate the cellular uptake of PNs and MNs in A549 human lung adenocarcinoma cell line, fluorescent probe coumarin-6 (C6) was encapsulated in the nanoparticles, in the same way as for the MH-loaded nanoparticles. The C6-loading of the two formulations was 0.2%.[28] Moreover, no more than 1% of the encapsulated C6 was released from the nanoparticles after 12 hours incubation in PBS pH 7.4 at 37°C. This guaranteed that the fluorescence signal detected in the cells was attributed to C6 encapsulated into the nanoparticles. Cells were seeded in 12-well plates at a density of 2×10^5 cells/well and incubated for 24 hours at 37°C to allow their attachment. To investigate whether nanoparticles were taken up through HA receptor-mediated endocytosis, cells were incubated with 10 mg/mL of free HA polymer for 1 hour prior to nanoparticles addition. The medium was replaced by 0.25 mg/mL of C6-PNs or C6-MNs diluted in serum-free cell culture medium (C6 content: 500 ng/mL).[29] After 2, 4, and 6 hours of incubation, the culture media were removed, and the cells were rinsed with PBS thrice. Subsequently, the cells were fixed with 4% formaldehyde for 10 minutes and observed under a fluorescence microscope (IX71; Olympus Corp, Tokyo, Japan)[30] and a Leica confocal laser scanning microscope (CLSM) (TCS SP5; Leica, Heidelberg, Germany).

Flow cytometry

The quantitative measurement of C6 fluorescence intensity was conducted using BD FACSCalibur FCM. The intracellular uptake was conducted as described in the previous section. After designated time intervals, the culture medium was removed and all cell samples were washed with PBS for three times. The cells were harvested by trypsinization and collected by centrifugation. Following supernatant aspiration, the cells were washed with PBS twice and then resuspended in 0.5 mL of PBS prior to fluorescent intensity measurements.[31]

Exploring uptake pathways of PNs and MNs using endocytic inhibitors

In order to evaluate the effect of different endocytic inhibitors on the uptake of the polymeric nanoparticles, A549 cells were preincubated individually with the following inhibitors: 0.45 M sucrose,[32] 15 μg/mL nystatin,[33] 50 μM amiloride,[34] and 10 mg/mL HA. After preincubation for 1 hour, the nanoparticles were added and incubated for a further 2 hours. Subsequently, the cells were washed three times with cold PBS (pH 7.4), harvested, collected by centrifugation, and resuspended in PBS for FCM analysis (BD FACSCalibur). All measurements were performed in triplicate.

In vivo antitumor activity

The in vivo antitumor activity of the nanoparticles was evaluated in a subcutaneous S180 murine sarcoma model in nude mice. To set up the tumor xenograft model, mice were subcutaneously inoculated in the armpit with S180 cells (2×10^6 cells) suspended in 200 μL PBS.[35] When the tumor volume reached approximately 100 mm^3, at day 5 post-tumor inoculation, mice were randomly divided into six groups (n=7 for each group) as follows: 1) saline; 2) blank PNs; 3) blank MNs; 4) MH drug solution (15 mg/kg); 5) MH-PNs (15 mg/kg); and 6) MH-MNs (15 mg/kg). All groups were injected intravenously via the tail vein (noted as day 0). The therapy was continued five times, with a 1-day interval between two administrations. The rate of survival was calculated based on Kaplan–Meier plot. Tumor sizes were measured every other day. At 2 days after the last injections, two of the mice in each group were randomly chosen and sacrificed to prepare the tumor sections. Tumors were extirpated, washed thrice with saline, weighed, and then fixed in 10% formalin. Formalin-fixed tumors were embedded in paraffin blocks to prepare hematoxylin and eosin (HE)-stained tumor sections. Furthermore, in vivo tumor cell apoptosis was investigated by terminal deoxynucleotidyl transferase dUTP nick end labeling (TUNEL) assay using an apoptotic cell detection kit (KeyGen Biotech, Nanjing, People's Republic of China) following the manufacturer's protocol. The sections were then visualized under a fluorescence microscope (Olympus Corp). TUNEL-positive cells and the total number of cells were counted in ten randomly selected microscopic fields for each tumor tissue sample, and the apoptotic index was calculated by dividing the number of apoptotic cells (positive cells) by the total number of cells.

Statistical analysis

All experiments were repeated at least three times. The data are expressed as mean ± SD. Statistical analysis was performed using Student's *t*-test, and differences were judged to be significant at $P<0.05$.

Results and discussion

Effect of HA/BCA molar ratio on particle size

Redox radical emulsion polymerization, initiated by a redox system composed of a polysaccharide having a MW in the range of 10 to 50 kDa and Ce^{+4}, first developed by Passirani et al[36] has opened a new perspective in the development of new drug delivery systems with versatile properties. The particle size of HA-PBCA nanoparticles reported by He et al was mainly dependent on the MW of HA, the cerium ammonium nitrate concentration, and the HA to BCA ratio.[15] It is well know that small micelle size is expected to prevent uptake by the reticuloendothelial system and facilitates extravasation at leaky sites of capillaries, leading to passive accumulation in certain tissues, eg, tumors.[37] However, the particle size reported by the group was larger than 290 nm, which was not favorable for drug-targeting. Therefore, we herein report the preparation of HA-PBCA nanoparticles from low-molecular-weight HA (10 kDa), where both the concentration of cerium ammonium nitrate (0.8 mmol/L) and the reaction time (1 hour) were kept constant. As shown in Figure 2, the sizes of HA-PBCA nanoparticles prepared at

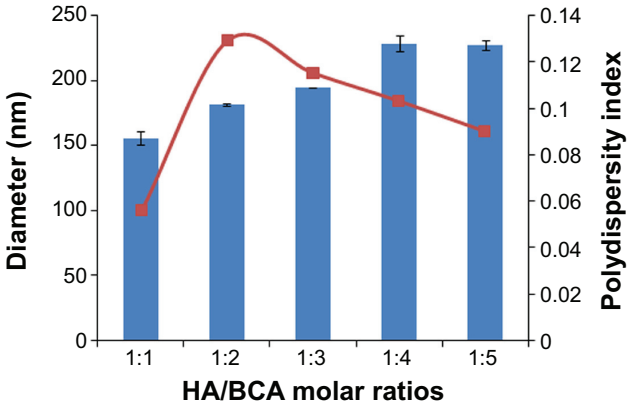

Figure 2 Effect of HA/BCA molar ratio on particle size.
Notes: HA-PBCA nanoparticles were prepared by radical emulsion polymerization from low molecular weight HA at a constant concentration of cerium ammonium nitrate (0.8 mmol/L) and 1 hour reaction time. Variation of nanoparticles diameter was evaluated as a function of HA/BCA molar ratio. Error bars refer to standard deviations, n=3.
Abbreviations: HA, hyaluronic acid; BCA, butyl cyanoacrylate; HA-PBCA, hyaluronic acid-poly(butyl cyanoacrylate).

different molar ratios were in the range of 155.7–228.9 nm, with high suspension turbidity, indicating that a large number of nanoparticles were formed. Increase in BCA amount did not remarkably influence the particle size of the nanoparticles; these results comply with those of a previous study.[38] Therefore, nanoparticles prepared with HA:BCA at a molar ratio of 1:1 were selected to conduct further experiments.

Critical aggregation concentration

Polymeric nanoparticles are prone to deaggregation upon dilution incurred in the biological environment. Therefore, CAC is considered as an important parameter to evaluate nanoparticles stability.[39] The CAC of HA-PBCA and HA-PBCA/TPGS could be accurately determined from the plot of the intensity ratio I_{338}/I_{333} as a function of the concentration of block copolymers (Figure 3). The CAC value of HA-PBCA was equal to 0.00501 mg/mL, which is comparatively lower than the CAC value of different types of HA-based block copolymers intended for the delivery of anticancer therapeutics, such as HA-poly(lactic-co-glycolic acid) (HA-PLGA) (CAC =0.0089 mg/mL).[40] Moreover, HA-PBCA/TPGS exhibited lower CAC value, of 0.00398 mg/mL, as compared with HA-PBCA, due to the π–π interactions induced by the aromatic rings of tocopherol (which have been identified as a CAC-lowering factor).[41] These results underlie the high stability and the ability of both PNs and MNs to maintain their integrity upon extreme dilution in the body.

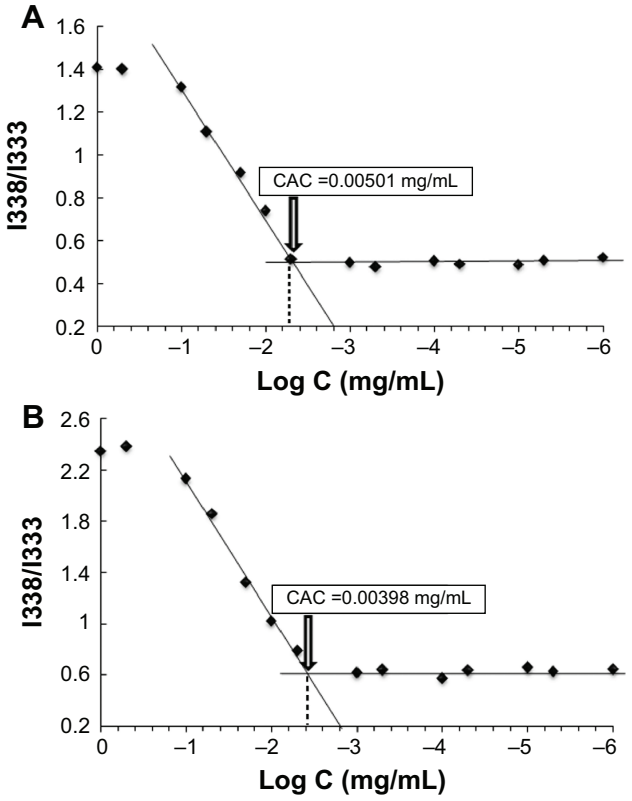

Figure 3 Plot of the intensity ratio (1338 nm/1333 nm) from pyrene emission spectra versus the logarithm of the concentration (Log C) of (**A**) HA-PBCA and (**B**) HA-PBCA/TPGS at pH 7.4.
Notes: The CAC value was determined as the point of intersection of two tangents drawn to the curve at high and low concentrations, respectively.
Abbreviations: CAC, critical aggregation concentration; HA-PBCA, hyaluronic acid-poly (butyl cyanoacrylate); TPGS, D-alpha-tocopheryl polyethylene glycol 1000 succinate.

Preparation and characterization of MH-loaded nanoparticles

In this study, self-assembled nanoparticles consisting of biocompatible HA and PBCA block copolymer were formed using a simple ultrasonic method. MH as a model hydrophobic drug was physically incorporated into the inner core of the polymeric nanoparticles. The characteristics of MH-PNs and MH-MNs, including DL, EE, and particle size, are summarized in Table 1. We found that the mean diameters of blank PNs and of MH-PNs were 155.7±5.1 nm and 170.36±2.21 nm, respectively, with a low polydispersity index, of about 0.056±0.013 and 0.130±0.089, respectively. Encapsulation of MH did not significantly increase the average size and size distribution of the PNs. As expected, the surface charge of MH-PNs was negative, with zeta potential of about –25.18±0.31, due to the presence of HA in the nanoparticles shell, which would prevent aggregation through

Table 1 Physical characterization of polymeric nanoparticles in PBS pH 7.4

Composition	TPGS % (w/v)	Particle size (nm)[a] by DLS	Particle size (nm)[a] by TEM	PDI[a]	Zeta potential (mV)[a]	EE%[a]	DL%[a]
HA-PBCA/MH (15:2.25)	0	170.36±2.21	134.78±6.15	0.130±0.089	–25.18±0.31	32.61±1.72	4.67±0.71
HA-PBCA/MH (15:2.25)	0.125	162.30±2.77	129.44±7.23	0.164±0.029	–27.46±0.17	61.58±2.35	7.26±0.46
HA-PBCA/MH (15:2.25)	0.25	134.73±1.85	120.83±5.89	0.125±0.065	–31.72±0.17	73.9±1.69	7.51±0.29

Note: [a]Data are expressed as mean ± SD (n=3).
Abbreviations: DL, drug-loading; DLS, dynamic light scattering; EE, entrapment efficiency; HA-PBCA, hyaluronic acid-poly(butyl cyanoacrylate); MH, morin hydrate; PBS, phosphate-buffered saline; PDI, polydispersity index; SD, standard deviation; TEM, transmission electron microscopy; TPGS, D-alpha-tocopheryl polyethylene glycol 1000 succinate.

electrostatic repulsion. The DL and the EE of MH-PNs were about 4.67%±0.71% and 32.61%±1.72%, respectively. Many studies have reported that the major factor influencing both the DL capacity and efficiency of block copolymer nanoparticles is the compatibility and the interactions between the drug and the core-forming block.[42] The relatively low EE of MH is due to the weak interactions between MH and PBCA core, leading to leakage of the drug into the dispersion medium during nanoparticle formation.[43] Furthermore, it was previously reported that drug molecules with small molecular weight, such as MH, have a faster diffusion coefficient and may thus escape the forming polymer network, leading to a low EE.[44] Aside from low polymer–drug compatibility and interactions, low efficiency may also be due to the high degree of interdigitation of the butyl chains in the core, which logically reduced the available space for MH and hampered its encapsulation.[29]

The addition of TPGS to HA-PBCA led to a slight decrease in the nanoparticles size (134.73±1.85) (Figure 4A), and increase in negative zeta potential (–31.72±0.17), thereby confirming the stabilizing ability of TPGS. Interestingly, the addition of TPGS resulted also in a significant increase in DL, proportional with the elevation in the TPGS feed ratio. The DL of MNs made of HA-PBCA and TPGS at the mass ratio of 1:0.5 (0.25% TPGS) was about 7.51%±0.29% compared with 4.67%±0.71% for the nanoparticle made of pure HA-PBCA. This can be explained by the fact that TPGS possesses a bulky shape and has large surface areas. Such characteristics make it a good emulsifier that can emulsify a wide range of hydrophobic drugs, including MH.[45] Gao et al further explained the increased EE resulting upon addition of TPGS to nanoparticles by more "loose" and "density" core structure because of the aromatic ring of TPGS, which may cause stronger hydrophobic interactions between drugs and polymers.[46]

Moreover, both MH-PNs and MH-MNs suspensions could be freeze-dried and properly redispersed in buffer solution under stirring and gentle sonication conditions. In addition, the MH-loaded nanoparticles presented an excellent colloidal stability over several months at 4°C, which is crucial regarding the storage stability of formulated MH. TEM studies (Figure 4B) showed that MH-loaded polymeric nanoparticles (MH-PNs and MH-MNs) displayed a uniform spherical morphology. The particle size obtained by TEM was smaller than that obtained by DLS due to the shrinkage of the nanoparticles during the drying process.[28]

DSC was employed to assess the physical status of MH inside the PNs and the MNs. The DSC thermograms (Figure 4C) of MH-PNs and MH-MNs exhibited endothermic peaks similar to those of blank nanoparticles, with absence of the characteristic peaks of MH, suggesting that MH was successfully encapsulated inside the lyophilized nanoparticles.

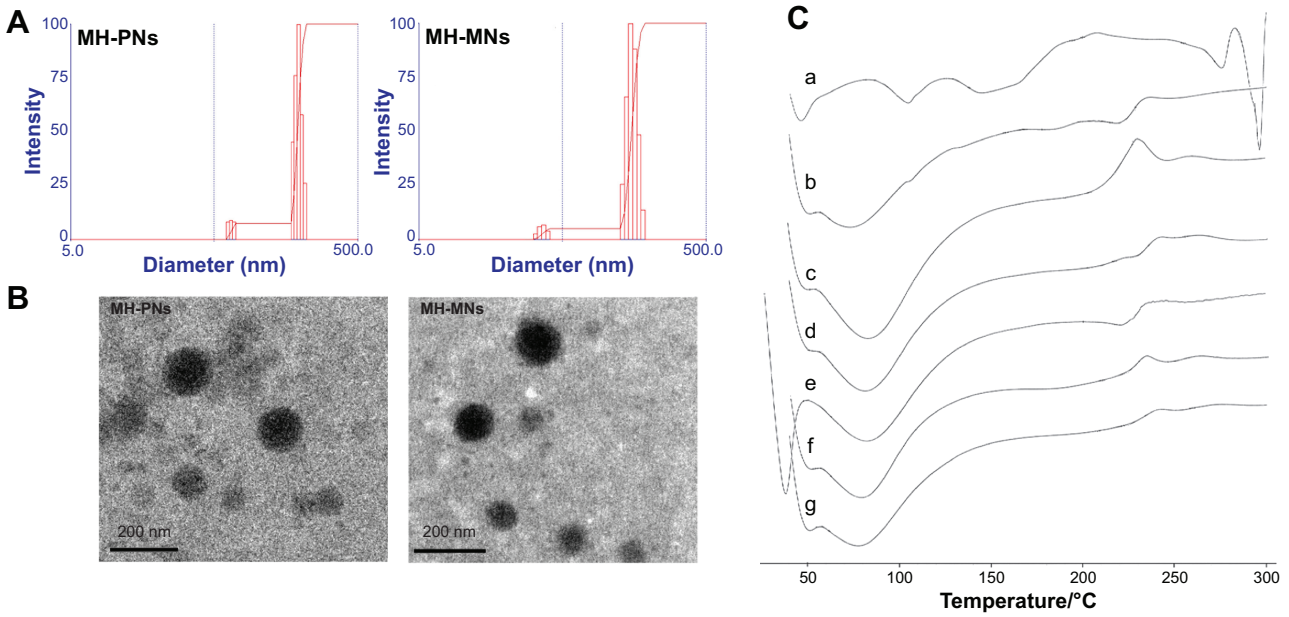

Figure 4 (**A**) Particle size distribution and (**B**) morphological characteristics of MH-PNs and MH-MNs, as determined by DLS and TEM, respectively. (**C**) DSC thermogram of (a) MH, (b) physical mixture of MH and HA-PBCA, (c) blank PNs, (d) MH-PNs, (e) physical mixture of MH, HA-PBCA and TPGS, (f) blank MNs, and (g) MH-MNs.
Abbreviations: DLS, dynamic light scattering; DSC, differential scanning calorimetry; HA-PBCA, hyaluronic acid-poly(butyl cyanoacrylate); MH-MNs, morin hydrate-loaded mixed nanoparticles; MH-PNs, morin hydrate-loaded plain nanoparticles; TEM, transmission electron microscopy; TPGS, D-alpha-tocopheryl polyethylene glycol 1000 succinate.

In vitro cytotoxicity studies

Figure 5A depicts the percentage of viable A549 cells incubated with blank nanoparticles for 72 hours. Empty PNs had no significant effect on the viability of A549 at concentrations ranging from 1 to 50 μg/mL. At higher concentrations, a small decrease in the cell viability was observed. In contrast, blank MNs achieved higher cytotoxic effect than blank PNs ($P<0.001$) due to the ability of TPGS to trigger the mitochondrial pathway of apoptosis in A549 cells.[47] To investigate whether blank nanoparticles could affect the viability of normal cells, the cytotoxicity was assessed in L02 cells by MTT assay for a period of 72 hours (Figure 5B). Both blank PNs and blank MNs did not show a significant toxicity against L02 cells, except at very high concentration in the case of blank MNs (500 mg/mL). This concentration is, however, much higher than the concentration needed for the half maximal inhibitory concentration (IC_{50}) of MH-MNs. Together, these findings revealed that TPGS may selectively exhibit chemotherapeutic effects against cancer cells without diminishing the cell viability of normal cells. Previous investigations have also reported the selective effect of TPGS for cancer growth inhibition.[22,48] A recent study has shown that the selective chemotherapeutic effects of TPGS may possibly be attributed to the downregulation of the antiapoptotic proteins survivin and Bcl-2, which are overexpressed in most cancer cells, with a greatly reduced expression in adult normal cells.[49,50] However, the exact mechanism responsible for this selectivity is not clear yet.

Previous study conducted by Manna et al using different cell lines including A549 indicated that morin suppresses the activation of NF-κB and NF-κB-regulated gene expression, leading to an enhancement of apoptosis.[51] The tumor specificity of morin was reported to be mainly exerted via both the 2′ and 4′ hydroxyl groups.[52] It was further found that morin-induced apoptosis in HL-60 cells was associated with elevated intracellular reactive oxygen species (ROS).[6]

Cytotoxicity was evaluated by the PI assay because of the interference of MH with the mitochondrial functions, leading to a false cytotoxicity evaluation by MTT assay. We found that the cytotoxic effect of MH was dose- and time-dependent. In compliance with previously published results, the significant apoptotic effect of MH only appeared after 72 hours.[4,6] Interestingly, the results shown in Figure 5C demonstrate that MH encapsulated in nanoparticles achieved higher cytotoxicity compared with free MH. This can be attributed to the fact that nanoparticles could be more

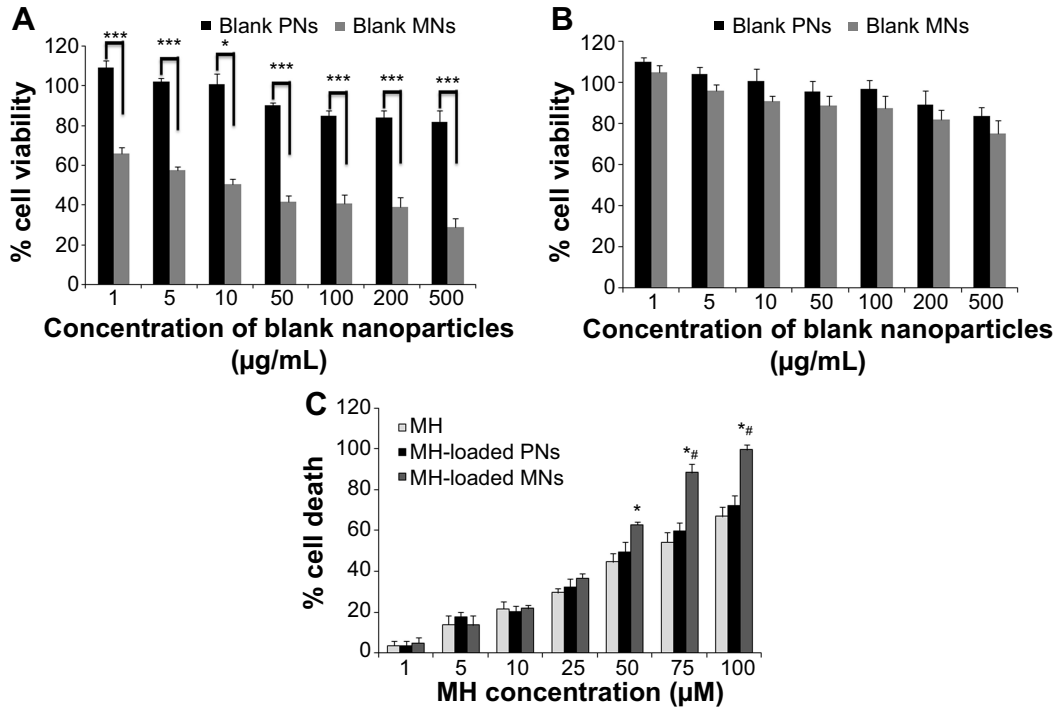

Figure 5 In vitro cytotoxicity studies.

Notes: In vitro cytotoxicity of blank PNs and blank MNs determined by MTT assay in (**A**) A549 cells and (**B**) L02 cells. A549 and L02 cells were incubated with different concentrations of blank nanoparticles for 72 hours. *$P<0.05$; ***$P<0.001$. (**C**) Cytotoxicity of free MH, MH-PNs, and MH-MNs determined by PI assay in A549 cells. Cell death was evaluated by PI assay as a function of MH concentration for 72 hours. *$P<0.05$ versus MH group and #$P<0.05$ versus MH-PNs group. Data represent mean ± SD (n=5).

Abbreviations: A549, human lung adenocarcinoma cell line; L02, human hepatic cell line; MH, morin hydrate; MH-MNs, morin hydrate-loaded mixed nanoparticles; MH-PNs, morin hydrate-loaded plain nanoparticles; MNs, mixed nanoparticles; MTT, 3-[4,5-dimethylthiazol-2-yl]-2,5-diphenyl-tetrazolium bromide; PI, propidium iodine; PNs, plain nanoparticles; SD, standard deviation.

efficiently taken up via CD44 receptor-mediated endocytosis (hence delivering more MH into cells and resulting in an increased cytotoxicity compared with the passive diffusion of free MH).[53] After 72 hours of incubation, the IC_{50} of free MH against A549 cells was 56.23 μM, whereas the IC_{50} values of MH-PNs and MH-MNs were 45.76 μM and 28.89 μM, respectively. Moreover, MH-MNs showed a higher cytotoxic potency compared with MH-PNs. The synergistic antitumor activity of TPGS in the presence of MH is due to its ability to induce ROS-generation and apoptosis.[54,55] Besides the two above reasons, another factor contributing to the improved cytotoxicity of MH-MNs over MH-PNs and free MH is the ability of both TPGS and MH to inhibit the P-gp protein expressed in A549 cells and reduce drug efflux.[56–58]

Cellular uptake

HA-PBCA forms a core–shell structure block copolymer that can self-assemble into polymeric micelles or nanoparticles. The advantages of this structure are that hydrophobic MH can be encapsulated in the core, whereas the shell composed of HA can shield the nanoparticles from the attack of plasma proteins. Moreover, the HA segment exposed toward the surface of the nanoparticles can target CD44 and RHAMM that are excessively expressed in tumor cells. Although MH was reported to display some fluorescence either by itself or when forming metal complexes,[59–61] we found that its fluorescence in A549, HepG2, and HeLa cells within the 1–50 μg/mL concentration range was negligible. MH fluorescence-quenching can be due to interactions with proteins and need further investigation.[62] To address the concept of HA receptor-targeting, C6 as a model fluorescent molecule was entrapped in the nanoparticles and the endocytosis kinetics were monitored by fluorescence microscopy. C6 fluorescence intensity was further quantified by FCM at different time points. A549 cells overexpressing CD44 receptors were used for cellular uptake evaluation.[63]

As shown in Figure 6A and B, both fluorescence microscopy and CLSM revealed bright green fluorescence signals in the cytoplasm of A549 cells, which was attributed to C6, indicating that C6-incorporated nanoparticles successfully entered the cells. However, under the same conditions, the C6-loaded nanoparticles displayed remarkably higher intensity compared with free C6. The intracellular uptake was quantitatively analyzed by FCM, as seen in Figure 6C and D. The fluorescence intensities of C6-PNs and C6-MNs were approximately 6.79-fold and 15.5-fold higher, respectively, than that of free C6 after incubation for 4 hours. These results clearly suggest that C6-loaded nanoparticles internalized into cells via overexpressed CD44 receptors. In addition, the fluorescence signal gradually became stronger with extended incubation time, indicating that the intracellular uptake of the nanoparticles increased in a time-dependent manner. Moreover, reports indicate that HA is expected to interact with CD44 mainly through its carboxylates groups, which can engage into polyelectrolyte interactions with the positively charged domain of CD44 receptors.[55,64] Therefore, the high efficacy of cellular uptake in A549 may be due to the fact that the chemical modification of HA at the end of its chains left the carboxylates groups along the polysaccharide chain disposed to interact with the CD44 receptors.

The higher fluorescence intensity of C6-MNs implied higher intracellular uptake capabilities for these new MNs compared with PNs. Indeed, the cellular uptake study showed that mixed nanoparticles with TPGS displayed 2.25-fold and 2.28-fold higher cellular uptake compared with the ones without TPGS after 2 and 4 hours of incubation, respectively. We have previously demonstrated that TPGS could significantly increase the cellular uptake of TPGS-phospholipid-C6 micelles in A549 cells as compared with phospholipid-C6 complex, as a result of the TPGS absorption enhancement effect.[28] TPGS-emulsified, drug-loaded PLGA nanoparticles have also shown higher cellular uptake than emulsified poly(vinyl alcohol) (PVA) nanoparticles, due to biophysical interactions with the membrane.[65] Zhao and Yung have also demonstrated that the cellular uptake of PLGA-PEG-FOL mixed micelles with TPGS was higher compared with the ones without TPGS.[66] Our in vitro results also confirmed these previous findings.

To further elucidate the mechanism of internalization, a competitive experiment was performed by treating A549 cells with free soluble HA prior to incubation with the nanoparticles. As expected, both fluorescence microscopy and FCM demonstrated a decrease in the fluorescence intensity in tumor cells pretreated with HA compared with the untreated cells. This result suggests that free HA could competitively bind to CD44 receptors and thereby block the binding of C6-loaded nanoparticles to these receptors. However, the extent of the fluorescence intensity remained unchangeable with or without blocking when cells were incubated with free C6, which was taken up by passive diffusion or other energy-dependent mechanism.[67] These observations confirmed that the nanoparticles predominantly trafficked into cells via a receptor-mediated endocytosis pathway.

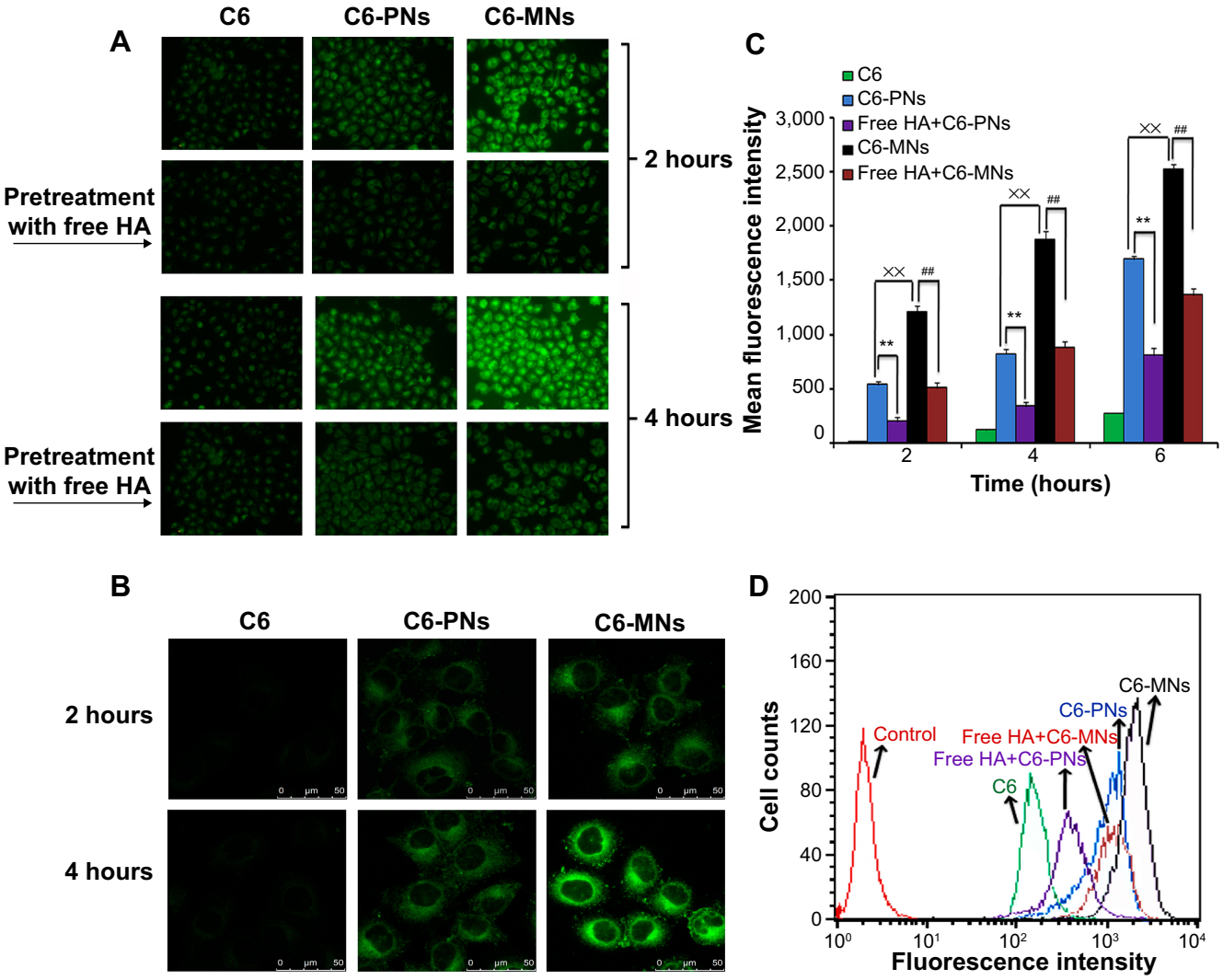

Figure 6 In vitro evaluation of cellular internalization.

Notes: (**A**) Cellular uptake of free C6, C6-PNs, and C6-MNs with and without pretreatment with free HA polymer, in A549 as a function of the incubation time (2 and 4 hours at 37°C). (**B**) Confocal microscopic images of A549 cells after incubation with free C6, C6-PNs, and C6-MNs for 2 and 4 hours. (**C**) Quantitative flow cytometric analysis of the intracellular uptake of C6, C6-PNs, and C6-MNs with and without pretreatment with free HA polymer in A549 cells for 2, 4, and 6 hours of incubation. $^{**,\#\#,\times\times}P<0.01$. (**D**) Flow cytometric curves of C6, C6-PNs, and C6-MNs with and without pretreatment with free HA polymer after 4 hours of incubation in A549 cells. Each analysis was generated by counting 10^4 cells. Results are expressed as the mean ± SD.

Abbreviations: C6, coumarin-6; C6-MNs, coumarin-6-loaded mixed nanoparticles; C6-PNs, coumarin-6-loaded plain nanoparticles; HA, hyaluronic acid; SD, standard deviation.

Exploring uptake pathways of nanoparticles

The elucidation of the exact intracellular uptake pathway of the nanoparticles remains challenging as some pathways are still insufficiently understood, and the functions of some proteins involved in cellular internalization are still uncertain.[68] The intracellular fate of nanoparticles is ultimately linked with the route of entry, which is dependent on the surface properties of the nanoparticles.[69] Endocytosis represents the major transport mechanism for nanomedicines across the membrane, including two major categories: phagocytosis, known as "cell eating", involving uptake of particles larger than 0.5 µm; and pinocytosis or "cell drinking" of fluid, solutes and suspensions containing small particles. Pinocytosis can be further subdivided into macropinocytosis, clathrin-dependent, caveolin-dependent, and clathrin/caveolin-independent pathways.[70,71]

In order to explore the cellular uptake pathway of PNs and MNs, an uptake inhibition study was conducted, by pretreating A549 cells with different chemical inhibitors, each specific for a particular endocytic pathway. Hypertonic sucrose, the most popular inhibitor of clathrin-mediated endocytosis, has been shown to prevent the proper assembly of clathrin lattices at the

plasma membrane.[72,73] Nystatin is a sterol-binding agent that disassembles caveolae and cholesterol in the membrane without affecting the clathrin-dependent internalization.[74] Amiloride is a specific inhibitor of macropinocytosis, by interfering with the Na^+/H^+ exchange protein in the plasma membrane.[75,76]

The results of the internalization of C6-PNs and C6-MNs in the presence of different pathway inhibitors are represented in Figure 7. A549 cells incubated with C6-PNs and C6-MNs without inhibitors were used as controls. Compared with the control groups, hypertonic sucrose solution reduced the cellular uptake of PNs and MNs by 36.84% and 44.93%, respectively. These observations provide strong evidence that the entry of these nanoparticles depends upon clathrin-mediated endocytosis. A slight decrease in the uptake of the nanoparticles after incubation with amiloride was observed, implying that macropinocytosis was partly involved in the uptake mechanism of these nanoparticles. The obtained results suggest that the internalization process occurred mainly via clathrin-mediated endocytosis, while a minor fraction could be internalized via macropinocytosis. Overall, the uptake mechanisms of the developed nanoparticles showed good correlations with the previously reported HA-based nanoparticles studies. In fact, both pH-responsive HA-g-poly(L-histidine) copolymer micelles and folate-conjugated HA-octadecyl (FA-HA-C18) copolymer, developed by Qiu et al and Liu et al respectively, internalized into cells mainly via clathrin-mediated endocytosis.[53,77]

In vivo antitumor activity

To confirm the antitumor potential of MH-loaded nanoparticles in vivo, the antitumor efficacy was evaluated in a subcutaneous S180 tumor xenograft model. As shown in Figure 8A, saline and blank PNs groups showed a rapid increase in tumor growth in S180 tumor-bearing mice over the whole period of the experiment. Meanwhile, groups treated with free MH and blank MNs exhibited a higher growth delay in comparison with the saline control group, which confirmed the antitumor effect of MH and TPGS. Interestingly, significant suppression of the tumor growth was observed during the treatment with MH-PNs and MH-MNs. In addition, MH-MNs had an evidently higher tumor inhibitory effect than other groups.

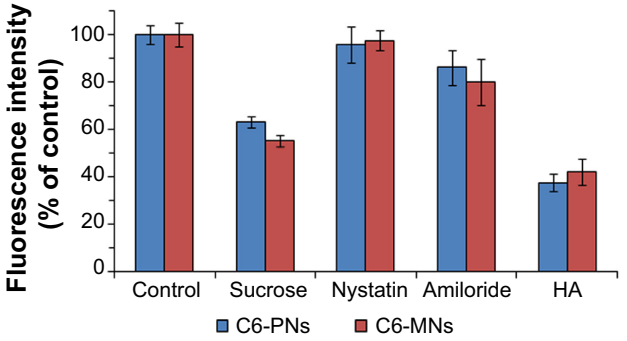

Figure 7 Effect of endocytic inhibitors on the internalization of C6-PNs and C6-MNs in A549 cells (n=3).

Notes: A549 cells were pretreated with 0.45 M sucrose, 15 μg/mL nystatin, 50 μM amiloride, and 10 mg/mL HA for 1 hour and then, treated with C6-PNs and C6-MNs for 2 hours at 37°C. A549 cells incubated with C6-PNs and C6-MNs without inhibitors were used as controls. The fluorescence intensity of each group was evaluated by FCM.

Abbreviations: C6-MNs, coumarin-6 loaded mixed nanoparticles; C6-PNs, coumarin-6 loaded plain nanoparticles; FCM, flow cytometry; HA, hyaluronic acid.

Figure 8B shows the Kaplan–Meier survival curves of S180 tumor-bearing mice injected with physiological saline, blank nanoparticles, free MH, and MH-loaded nanoparticles. All mice in the saline, blank PNs, and MH groups died within 20 days after initial treatment. The survival time of mice treated with blank MNs (24 days) turned out to be longer than that of MH-treated animals. Such superiority could be attributed to the prolonged circulation time and the targeting ability of blank MNs toward CD44 receptors, leading to a higher accumulation of TPGS in the tumor site compared with MH injection, which was eliminated more rapidly. In contrast, MH-PNs and MH-MNs contributed to prolonged survival time of the treated mice, with survival rates of 57% and 71% until day 20, respectively.

Besides attenuating the tumor growth, the median survival time of mice treated with MH-PNs and MH-MNs was significantly longer than that of mice treated with physiological saline, blank nanoparticles, and MH solution. The better survival rate of the groups administered with blank MNs and MH-loaded nanoparticles could be due to the targeting capability of HA as it increased the binding affinity to CD44 receptors in the tumor site. Indeed, the HA employed has a low molecular weight (10 kDa), long enough to bind to CD44 but too short to bind to the hyaluronan receptor for endocytosis (HARE) on liver sinusoidal endothelial cells, thus avoiding clearance by the liver.[78] The prolonged survival time obtained with MH-MNs over MH-PNs is mainly attributed to the anticancer activity of TPGS and to the synergistic combination of active targeting through HA and passive targeting through the EPR effect of TPGS, leading to more accumulation at the tumor site.

The improved antitumor efficacy of the different MH formulations in mice was further confirmed by the histopathology analysis. The representative HE-stained tumor sections from the different experimental groups of mice are displayed in Figure 8C. The groups injected with saline and blank PNs showed the typical pathological characteristics of tumor, such as closely packed tumor cells. The image showed a massive

cancer cell remission after the administration of MH, blank MNs, MH-PNs, and MH-MNs, which presents substantial evidence of the efficient antitumor activity of MH, TPGS, and MH-loaded nanoparticles in vivo. In particular, MH-MNs exhibited the most effective antitumor activity due to the synergistic anticancer effect of MH and TPGS, and combined passive and active targeting effects. The in vivo results were consistent with those obtained in vitro.

To analyze the degree to which MH-loaded nanoparticles induced apoptosis in vivo, we performed a TUNEL assay on tumor sections. As shown in Figure 8C, tumors from the MH-MNs-treated group exhibited more advanced cell apoptosis (TUNEL-positive nuclei are stained in dark brown) compared with the control-, blank nanoparticle-, and MH-PN-treated groups. Quantification of the TUNEL-positive spots (Figure 8D) showed that tumor sections from the groups

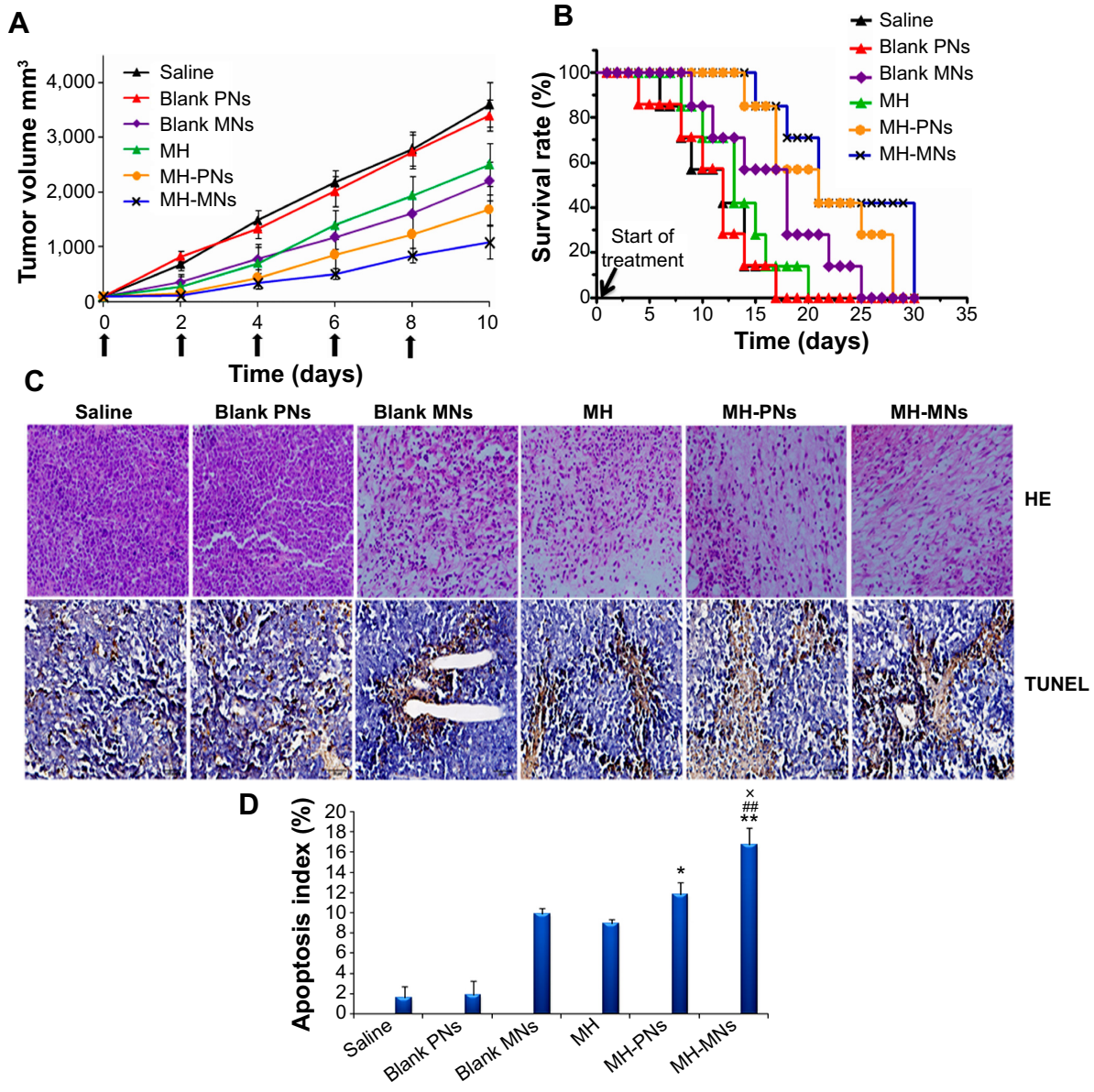

Figure 8 In vivo antitumor efficacy in S180 tumor-bearing nude mice.

Notes: (**A**) Tumor volume changes as a function of time after intravenous injection of saline, blank PNs, blank MNs, free MH, MH-PNs, and MH-MNs. The concentration of blank nanoparticles used was equal to the concentration of MH-loaded nanoparticles. Throughout the study, tumors were measured using a digital caliper, and tumor volumes were calculated from the formula: $V = 1/2$ (length × width^2). The arrows signify the time of intravenous administration. Data are expressed as mean ± SD (n=7). (**B**) Kaplan–Meier survival curves of tumor-bearing mice. The survival of mice was recorded since the first day of injection. (**C**) Representative images of tumor sections separated from mice after HE and TUNEL staining. (**D**) The apoptosis index is shown as a percentage of TUNEL-positive cells. $^{*}P<0.05$ and $^{**}P<0.01$ versus MH group, $^{\#\#}P<0.01$ versus blank MNs group, $^{\times}P<0.05$ versus MH-PNs.

Abbreviations: HE, hematoxylin and eosin; MH, morin hydrate; MH-MNs, morin hydrate-loaded mixed nanoparticles; MH-PNs, morin hydrate-loaded plain nanoparticles; MNs, mixed nanoparticles; PNs, plain nanoparticles; SD, standard deviation; TUNEL, terminal deoxynucleotidyl transferase dUTP nick end labeling.

treated with blank MNs or MH contained 9.92% and 8.94% positive spots, respectively. The number of TUNEL-positive cells increased to 11.82% in the group treated with MH-PNs and, more importantly, to 16.67% in the group treated with MH-MNs, demonstrating that MH-MNs induce apoptosis and necrosis in tumor tissue at a much higher level than that observed in the other groups.

Conclusion

In this study, HA-PBCA was synthesized through redox radical emulsion polymerization to encapsulate the anticancer drug MH for specific targeting of CD44-overexpressing cancer cells. TPGS was further mixed with HA-PBCA during the self-assembly process in order to enhance the therapeutic efficacy of MH, which possesses a high IC_{50} value. The prepared PNs and MNs displayed a low CAC, a small spherical morphology, and a reasonable DL. MH-MNs exhibited more potent cytotoxic effect towards A549 cells compared with MH-PNs and MH solution, mainly due to the synergistic effect of the combination of TPGS with MH in one delivery system. Furthermore, the newly developed nanoparticulate system demonstrated an excellent cellular uptake in A549 cells, with mixed nanoparticles showing higher cellular uptake compared with their counterparts without TPGS. Endocytosis inhibition studies revealed that the nanoparticles were internalized mainly through clathrin-mediated endocytosis. Moreover, the intravenous administration of MH-loaded nanoparticle into S180 tumor-bearing mice resulted in a significant reduction of tumor volume. All these results suggest that the combination chemotherapy of MH and TPGS as well as tumor-targeted delivery using HA-based polymeric nanoparticles can be successfully utilized as an effective treatment for cancer.

Acknowledgment

The authors wish to thank Mrs Kaylie Towne from Western Michigan University for reading and improving the manuscript.

Disclosure

The authors report no conflicts of interest in this work.

References

1. Zhang J, Peng Q, Shi S, et al. Preparation, characterization, and in vivo evaluation of a self-nanoemulsifying drug delivery system (SNEDDS) loaded with morin-phospholipid complex. *Int J Nanomedicine*. 2011;6:3405–3414.
2. Gopal JV. Morin Hydrate: Botanical origin, pharmacological activity and its applications: A mini-review. *Pharmacognosy Journal*. 2013; 5(3):123–126.
3. Sivaramakrishnan V, Devaraj SN. Morin fosters apoptosis in experimental hepatocellular carcinogenesis model. *Chem Biol Interact*. 2010;183(2):284–292.
4. Romero I, Páez A, Ferruelo A, Luján M, Berenguer A. Polyphenols in red wine inhibit the proliferation and induce apoptosis of LNCaP cells. *BJU Int*. 2002;89(9):950–954.
5. Zhang S, Yang X, Morris ME. Flavonoids are inhibitors of breast cancer resistance protein (ABCG2)-mediated transport. *Mol Pharmacol*. 2004;65(5):1208–1216.
6. Kuo HM, Chang LS, Lin YL, et al. Morin inhibits the growth of human leukemia HL-60 cells via cell cycle arrest and induction of apoptosis through mitochondria dependent pathway. *Anticancer Res*. 2007;27(1A):395–405.
7. Waddad AY, Abbad S, Yu F, et al. Formulation, characterization and pharmacokinetics of Morin hydrate niosomes prepared from various non-ionic surfactants. *Int J Pharm*. 2013;456(2):446–458.
8. Zhang L, Yao J, Zhou J, Wang T, Zhang Q. Glycyrrhetinic acid-graft-hyaluronic acid conjugate as a carrier for synergistic targeted delivery of antitumor drugs. *Int J Pharm*. 2013;441(1–2):654–664.
9. Li J, Huo M, Wang J, et al. Redox-sensitive micelles self-assembled from amphiphilic hyaluronic acid-deoxycholic acid conjugates for targeted intracellular delivery of paclitaxel. *Biomaterials*. 2012;33(7):2310–2320.
10. Jiang T, Zhang Z, Zhang Y, et al. Dual-functional liposomes based on pH-responsive cell-penetrating peptide and hyaluronic acid for tumor-targeted anticancer drug delivery. *Biomaterials*. 2012; 33(36):9246–9258.
11. Yeo TK, Nagy JA, Yeo KT, Dvorak HF, Toole BP. Increased hyaluronan at sites of attachment to mesentery by CD44-positive mouse ovarian and breast tumor cells. *Am J Pathol*. 1996;148(6):1733–1740.
12. Poon Z, Lee JB, Morton SW, Hammond PT. Controlling in vivo stability and biodistribution in electrostatically assembled nanoparticles for systemic delivery. *Nano Lett*. 2011;11(5):2096–2103.
13. Pouyani T, Prestwich GD. Functionalized derivatives of hyaluronic acid oligosaccharides: drug carriers and novel biomaterials. *Bioconjugate Chem*. 1994;5(4):339–347.
14. Lee H, Lee K, Park TG. Hyaluronic acid-paclitaxel conjugate micelles: synthesis, characterization, and antitumor activity. *Bioconjug Chem*. 2008;19(6):1319–1325.
15. He M, Zhao Z, Yin L, Tang C, Yin C. Hyaluronic acid coated poly(butyl cyanoacrylate) nanoparticles as anticancer drug carriers. *Int J Pharm*. 2009;373(1–2):165–173.
16. Huang X, Xiao Y, Lang M. Self-assembly of pH-sensitive mixed micelles based on linear and star copolymers for drug delivery. *J Colloid Interface Sci*. 2011;364(1):92–99.
17. Dou J, Zhang H, Liu X, Zhang M, Zhai G. Preparation and evaluation in vitro and in vivo of docetaxel loaded mixed micelles for oral administration. *Colloids Surf B Biointerfaces*. 2014;114:20–27.
18. Wu SH, Hopkins WK. Characteristics of d-α-tocopheryl PEG1000 succinate for applications as an absorption enhancer in drug delivery systems. *Pharm Tech*. 1999;23:52–68.
19. Saxena V, Hussain MD. Poloxamer 407/TPGS mixed micelles for delivery of gambogic acid to breast and multidrug-resistant cancer. *Int J Nanomedicine*. 2012;7:713–721.
20. Yan A, Von Dem Bussche A, Kane AB, Hurt RH. Tocopheryl polyethylene glycol succinate as a safe, antioxidant surfactant for processing carbon nanotubes and fullerenes. *Carbon N Y*. 2007;45(13):2463–2470.
21. Zhang Z, Tan S, Feng SS. Vitamin E TPGS as a molecular biomaterial for drug delivery. *Biomaterials*. 2012;33(19):4889–4906.
22. Zhao H, Yung LY. Addition of TPGS to folate-conjugated polymer micelles for selective tumor targeting. *J Biomed Mater Res A*. 2009; 91(2):505–518.
23. Muthu MS, Kulkarni SA, Raju A, Feng SS. Theranostic liposomes of TPGS coating for targeted co-delivery of docetaxel and quantum dots. *Biomaterials*. 2012;33(12):3494–3501.
24. Jiang L, Li X, Liu L, Zhang Q. Thiolated chitosan-modified PLA-PCL-TPGS nanoparticles for oral chemotherapy of lung cancer. *Nanoscale Res Lett*. 2013;8(1):66.

25. Zheng Y, Chen H, Zeng X, et al. Surface modification of TPGS-b-(PCL-ran-PGA) nanoparticles with polyethyleneimine as a co-delivery system of TRAIL and endostatin for cervical cancer gene therapy. *Nanoscale Res Lett*. 2013;8(1):161.
26. Pal S, Ghosh S, De P. Synthesis via RAFT polymerization of thermo- and pH-responsive random copolymers containing cholic acid moieties and their self-assembly in water. *Polym Chem*. 2014;5(4):1275–1284.
27. Zhang L, Mizumoto K, Sato N, et al. Quantitative determination of apoptotic death in cultured human pancreatic cancer cells by propidium iodide and digitonin. *Cancer Lett*. 1999;142(2):129–137.
28. Munyendo WL, Zhang Z, Abbad S, et al. Micelles of TPGS modified apigenin phospholipid complex for oral administration: preparation, in vitro and in vivo evaluation. *J Biomed Nanotechnol*. 2013;9(12):2034–2047.
29. Ouahab A, Cheraga N, Onoja V, Shen Y, Tu J. Novel pH-sensitive charge-reversal cell penetrating peptide conjugated PEG-PLA micelles for docetaxel delivery: in vitro study. *Int J Pharm*. 2014;466(1–2):233–245.
30. Hou L, Yao J, Zhou J, Zhang Q. Pharmacokinetics of a paclitaxel-loaded low molecular weight heparin-all-trans-retinoid acid conjugate ternary nanoparticulate drug delivery system. *Biomaterials*. 2012;33(21):5431–5440.
31. Kim GT, Lee SH, Kim JI, Kim YM. Quercetin regulates the sestrin 2-AMPK-p38 MAPK signaling pathway and induces apoptosis by increasing the generation of intracellular ROS in a p53-independent manner. *Int J Mol Med*. 2014;33(4):863–869.
32. Heuser JE, Anderson RG. Hypertonic media inhibit receptor-mediated endocytosis by blocking clathrin-coated pit formation. *J Cell Biol*. 1989;108(2):389–400.
33. Yang H, Lou C, Xu M, Wu C, Miyoshi H, Liu Y. Investigation of folate-conjugated fluorescent silica nanoparticles for targeting delivery to folate receptor-positive tumors and their internalization mechanism. *Int J Nanomedicine*. 2011;6:2023–2032.
34. Jiang L, Li X, Liu L, Zhang Q. Cellular uptake mechanism and intracellular fate of hydrophobically modified pullulan nanoparticles. *Int J Nanomedicine*. 2013;8:1825–1834.
35. Wu D, Gao Y, Chen L, et al. Anti-tumor effects of a novel chimeric peptide on S180 and H22 xenografts bearing nude mice. *Peptides*. 2010;31(5):850–864.
36. Passirani C, Ferrarini L, Barratt G, Devissaguet JP, Labarre D. Preparation and characterization of nanoparticles bearing heparin or dextran covalently-linked to poly(methyl methacrylate). *J Biomater Sci Polym Ed*. 1999;10(1):47–62.
37. Lavasanifar A, Samuel J, Kwon GS. Poly(ethylene oxide)-block-poly(L-amino acid) micelles for drug delivery. *Adv Drug Deliv Rev*. 2002;54(2):169–190.
38. Bertholon-Rajot I, Labarre D, Vauthier C. Influence of the initiator system, cerium–polysaccharide, on the surface properties of poly(isobutylcyanoacrylate) nanoparticles. *Polymer*. 2005;46(4):1407–1415.
39. Dahmani FZ, Yang H, Zhou J, Yao J, Zhang T, Zhang Q. Enhanced oral bioavailability of paclitaxel in pluronic/LHR mixed polymeric micelles: preparation, in vitro and in vivo evaluation. *Eur J Pharm Sci*. 2012;47(1):179–189.
40. Jeong YI, Kim do H, Chung CW, et al. Self-assembled nanoparticles of hyaluronic acid/poly(DL-lactide-co-glycolide) block copolymer. *Colloids Surf B Biointerfaces*. 2012;90:28–35.
41. Duhem N, Rolland J, Riva R, et al. Tocol modified glycol chitosan for the oral delivery of poorly soluble drugs. *Int J Pharm*. 2012;423(2):452–460.
42. Allen C, Maysinger D, Eisenberg A. Nano-engineering block copolymer aggregates for drug delivery. *Colloids Surf B Biointerfaces*. 1999;16(1–4):3–27.
43. Diao YY, Li HY, Fu YH, et al. Doxorubicin-loaded PEG-PCL copolymer micelles enhance cytotoxicity and intracellular accumulation of doxorubicin in adriamycin-resistant tumor cells. *Int J Nanomedicine*. 2011;6:1955–1962.
44. Graf A, Krauel-Göllner K, Rades T. Poly(alkyl cyanoacrylate) nanoparticles for drug delivery and vaccine development. In: Fanun M, editor. *Colloids in Drug Delivery*. Boca Raton, FL: CRC Press; 2013:99–136.
45. Mu L, Feng SS. Vitamin E TPGS used as emulsifier in the solvent evaporation/extraction technique for fabrication of polymeric nanospheres for controlled release of paclitaxel (Taxol). *J Control Release*. 2002;80(1–3):129–144.
46. Gao Y, Li LB, Zhai G. Preparation and characterization of Pluronic/TPGS mixed micelles for solubilization of camptothecin. *Colloids Surf B Biointerfaces*. 2008;64(2):194–199.
47. Constantinou C, Papas A, Constantinou AI. Vitamin E and cancer: An insight into the anticancer activities of vitamin E isomers and analogs. *Int J Cancer*. 2008;123(4):739–752.
48. Pooja D, Kulhari H, Singh MK, Mukherjee S, Rachamalla SS, Sistla R. Dendrimer-TPGS mixed micelles for enhanced solubility and cellular toxicity of taxanes. *Colloids Surf B Biointerfaces*. 2014;121:461–468.
49. Neophytou CM, Constantinou C, Papageorgis P, Constantinou AI. D-alpha-tocopheryl polyethylene glycol succinate (TPGS) induces cell cycle arrest and apoptosis selectively in Survivin-overexpressing breast cancer cells. *Biochem Pharmacol*. 2014;89(1):31–42.
50. O'Driscoll L, Linehan R, Clynes M. Survivin: role in normal cells and in pathological conditions. *Curr Cancer Drug Targets*. 2003;3(2):131–152.
51. Manna SK, Aggarwal RS, Sethi G, Aggarwal BB, Ramesh GT. Morin (3,5,7,2′,4′-Pentahydroxyflavone) abolishes nuclear factor-kappaB activation induced by various carcinogens and inflammatory stimuli, leading to suppression of nuclear factor-kappaB-regulated gene expression and up-regulation of apoptosis. *Clin Cancer Res*. 2007;13(7):2290–2297.
52. Brown J, O'Prey J, Harrison PR. Enhanced sensitivity of human oral tumours to the flavonol, morin, during cancer progression: involvement of the Akt and stress kinase pathways. *Carcinogenesis*. 2003;24(2):171–177.
53. Qiu L, Li Z, Qiao M, et al. Self-assembled pH-responsive hyaluronic acid-g-poly((L)-histidine) copolymer micelles for targeted intracellular delivery of doxorubicin. *Acta Biomater*. 2014;10(5):2024–2035.
54. Jiang L, Li X, Liu L, Zhang Q. Thiolated chitosan-modified PLA-PCL-TPGS nanoparticles for oral chemotherapy of lung cancer. *Nanoscale Res Lett*. 2013;8(1):66.
55. Zaki NM. Augmented cytotoxicity of hydroxycamptothecin-loaded nanoparticles in lung and colon cancer cells by chemosensitizing pharmaceutical excipients. *Drug Deliv*. 2014;21(4):265–275.
56. Youk HJ, Lee E, Choi MK, et al. Enhanced anticancer efficacy of alpha-tocopheryl succinate by conjugation with polyethylene glycol. *J Control Release*. 2005;107(1):43–52.
57. Campbell L, Abulrob AN, Kandalaft LE, et al. Constitutive expression of p-glycoprotein in normal lung alveolar epithelium and functionality in primary alveolar epithelial cultures. *J Pharmacol Exp Ther*. 2003;304(1):441–452.
58. Salomon JJ, Ehrhardt C. Nanoparticles attenuate P-glycoprotein/MDR1 function in A549 human alveolar epithelial cells. *Eur J Pharm Biopharm*. 2011;77(3):392–397.
59. Wang X, Hwang SY, Cong WT, Jin LT, Choi JK. Phosphoprotein staining for sodium dodecyl sulfate-polyacrylamide gel electrophoresis using fluorescent reagent morin hydrate. *Anal Biochem*. 2013;435(1):19–26.
60. Panhwar QK, Memon S, Bhanger MI. Synthesis, characterization, spectroscopic and antioxidation studies of Cu(II)–morin complex. *J Mol Struct*. 2010;967(1–3):47–53.
61. Song Y, Kang J, Zhou J, et al. Study on the fluorescence spectra and electrochemical behavior of ZnL2 and Morin with DNA. *Spectrochim Acta A Mol Biomol Spectrosc*. 2000;56A(12):2491–2497.
62. Wang F, Huang W, Miao X, Tang B. Characterization and analytical application of Morin – bovine serum albumin system by spectroscopic approaches. *Spectrochim Acta A Mol Biomol Spectrosc*. 2012;99:373–378.

63. Ganesh S, Iyer AK, Morrissey DV, Amiji MM. Hyaluronic acid based self-assembling nanosystems for CD44 target mediated siRNA delivery to solid tumors. *Biomaterials*. 2013;34(13):3489–3502.
64. Peach RJ, Hollenbaugh D, Stamenkovic I, Aruffo A. Identification of hyaluronic acid binding sites in the extracellular domain of CD44. *J Cell Biol*. 1993;122(1):257–264.
65. Mu L, Seow PH. Application of TPGS in polymeric nanoparticulate drug delivery system. *Colloids Surf B Biointerfaces*. 2006;47(1):90–97.
66. Zhao H, Yung LY. Addition of TPGS to folate-conjugated polymer micelles for selective tumor targeting. *J Biomed Mater Res A*. 2009; 91(2):505–518.
67. Wang Y, Guo M, Lu Y, et al. Alpha-tocopheryl polyethylene glycol succinate-emulsified poly(lactic-co-glycolic acid) nanoparticles for reversal of multidrug resistance in vitro. *Nanotechnology*. 2012;23 (49):495103.
68. Kou L, Sun J, Zhai Y, He Z. The endocytosis and intracellular fate of nanomedicines: Implication for rational design. *AJPS*. 2013;8(1): 1–10.
69. Niu L, Panyam J. Intracellular trafficking of nanoparticles: Implication for therapeutic efficacy of the encapsulated drug. In: Yeo Y, editor. *Nanoparticulate Drug Delivery Systems: Strategies, Technologies, and Applications*. New York, NY: John Wiley & Son; 2013:261–280.
70. Iversen TG, Skotland T, Sandvig K. Endocytosis and intracellular transport of nanoparticles: Present knowledge and need for future studies. *Nano Today*. 2011;6(2):176–185.
71. Liu BR, Lo SY, Liu CC, et al. Endocytic trafficking of nanoparticles delivered by cell-penetrating peptides comprised of nona-arginine and a penetration accelerating sequence. *PLoS One*. 2013;8(6):e67100.
72. Blitzer JT, Nusse R. A critical role for endocytosis in Wnt signaling. *BMC Cell Biol*. 2006;7:28.
73. Ivanov AI. Pharmacological inhibition of endocytic pathways: is it specific enough to be useful? *Methods Mol Biol*. 2008;440:15–33.
74. Zhu XD, Zhuang Y, Ben JJ, et al. Caveolae-dependent endocytosis is required for class A macrophage scavenger receptor-mediated apoptosis in macrophages. *J Biol Chem*. 2011;286(10):8231–8239.
75. Khalil IA, Kogure K, Akita H, Harashima H. Uptake pathways and subsequent intracellular trafficking in nonviral gene delivery. *Pharmacol Rev*. 2006;58(1):32–45.
76. Koivusalo M, Welch C, Hayashi H, et al. Amiloride inhibits macropinocytosis by lowering submembranous pH and preventing Rac1 and Cdc42 signaling. *J Cell Biol*. 2010;188(4):547–563.
77. Liu Y, Sun J, Cao W, et al. Dual targeting folate-conjugated hyaluronic acid polymeric micelles for paclitaxel delivery. *Int J Pharm*. 2011; 421(1):160–169.
78. Upadhyay KK, Le Meins JF, Misra A, et al. Biomimetic doxorubicin loaded polymersomes from hyaluronan-block-poly(gamma-benzyl glutamate) copolymers. *Biomacromolecules*. 2009;10(10):2802–2808.